# Role of transverse magnetic fields in electromagnetically induced absorption for elliptically polarized light

J. Dimitrijević,* A. Krmpot, M. Mijailović, D. Arsenović, B. Panić, Z. Grujić, and B. M. Jelenković
*Institute of Physics, Pregrevica 118, 11080 Belgrade, Serbia*
(Received 20 August 2007; published 16 January 2008)

Using the closed $F_g \rightarrow F_e = F_g + 1$ $D2$ line transition of Rb atoms, we report experimental and numerical evidence of influence of additional transverse magnetic field when examining electromagnetically induced absorption (EIA) in the Hanle configuration. The effect was analyzed with two directions of additional magnetic field and in the cases of excitation with linear, elliptical, and circular laser light polarization. The transverse magnetic field brings substantial differences in the resonance line shape, amplitude, and width. Our theoretical model includes Doppler broadening. Numerical solutions of our theoretical model are in good agreement with experimental results. This analysis points out the importance of the presence of stray magnetic fields when studying EIA.

DOI: 10.1103/PhysRevA.77.013814 PACS number(s): 42.50.Gy

## I. INTRODUCTION

Electromagnetically induced transparency (EIT) [1,2] and electromagnetically induced absorption (EIA) [3–6] occur due to the same processes, optical pumping and coherences. These are laser induced processes between hyperfine levels of ground and excited states, or between Zeeman sublevels of two hyperfine levels. Atomic schemes required for EIT and EIA are different—$\Lambda$-atomic schemes, and $F_g \geq F_e$, are necessary for the EIT, while $V$-atomic schemes, and $0 < F_g < F_e$, are required for EIA [7]. Manifestations of EIT and EIA are also opposite: narrow transmission resonance (fluorescence dip) occurs in EIT media, while narrow absorption resonance (fluorescence gain) occurs in EIA media. Note that EIT is a manifestation of coherent population trapping (CPT) [8] and one way of observing CPT [9,10]. Depending on the configuration, i.e., the direction of light polarization vs the direction of an external magnetic field, both effects can be explained by optical pumping if a laser electrical vector is along an external magnetic field or by coherence if a magnetic vector is along the light propagation [7,11–13]. While coherences in the case of EIT are formed between lower (long-lived) levels, coherences in EIA are induced between upper levels of the $V$ scheme, subsequently transferred via spontaneous emission to lower hyperfine levels.

Steep dispersion at EIT and EIA resonances leads to the fascinating change of group velocity of light propagating through a gas media. Recent techniques have enabled extreme control over group velocities, giving ultraslow or "stopped" light in EIT medium [14–16] or fast light, in EIA medium [5,17–19]. These works promise practical applications such as controllable optical delay lines, data storage, and applications for quantum information. Strong dependence of these resonances on external magnetic field opens possibilities for the new high precision magnetometers [20,21]. Studying the dependence of resonance shapes, linewidths, and amplitudes, as functions of experimental parameters, such as laser polarization and magnetic fields, are then of great interest. Knowledge and understanding of how these parameters influence sub-Doppler wide resonances are important for developing or improving precision devices based on CPT and EIA.

EIT and EIA are mainly studied in a Doppler broadened media, by measuring or calculating laser transmission or fluorescence. Measurements are made by using either a probe-pump or a Hanle configuration. In the latter, a single laser excites a two-level atom while external magnetic scanning field $\vec{B}_{\text{scan}}$ varies around zero. External magnetic field $\vec{B}_{\text{scan}}$ is directed along propagation of laser light (direction of $\vec{k}$). In a typical setup, transverse $\vec{B}_{\text{trans}}$ (in respect to laser light propagation) magnetic field is minimized and its effects on the results are neglected or ignored.

Studies on CPT and EIT are more comprehensive than on EIA. Recently, influence of transverse magnetic fields on the amplitude and linewidths of the CPT resonances, observed in fluorescence, and of the EIT, observed in the laser transmission, were investigated in Rb, for the excitation with linear, circular, and elliptical laser light polarization [22]. It is shown that transverse magnetic field enhances or reduces (and even eliminates) CPT (EIT) depending on the orientation of this magnetic field with respect to the laser polarization. CPT resonances in Cs were studied with laser light having different elliptical polarization and for a few values of additional magnetic field perpendicular to a scanning magnetic field [23]. Both works [22,23] show strong variation of the amplitude of induced absorption gain for the circularly polarized laser light in the presence of transverse magnetic fields with components perpendicular to the laser propagation. Renzoni *et al.* [24], have shown that transverse magnetic field enhances narrow fluorescence gain (EIA) of circularly polarized laser, near zero values of scanning magnetic field. Studies of the behavior of EIA with interacting laser light of different ellipticity include works of Alzetta *et al.* [25], who showed different Hanle wave forms and signs of the fluorescence resonance for linearly and circularly polarized laser light. The fact that they were able to see the resonance (fluorescence dip) was theoretically explained to be due to imperfect circularly polarized light. The effect of the laser ellipticity, on EIA amplitudes and widths, in the presence of Doppler broadening, was recently studied by Brazhnikov [26] and of the intensity by Mijailović [27].

*jelenad@phy.bg.ac.yu

 

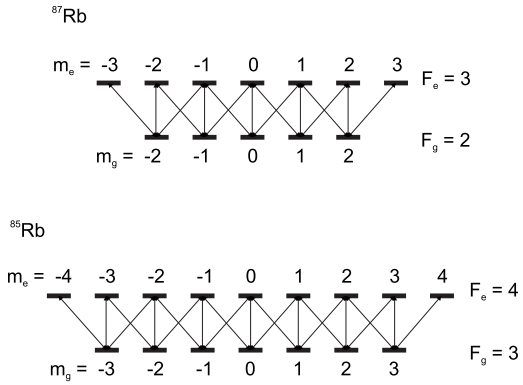


FIG. 1. Level diagrams for the $F_g=2\rightarrow F_e=3$ transition of $^{87}$Rb (up) and $F_g=3\rightarrow F_e=4$ transition of $^{85}$Rb (down). Lines connecting Zeeman sublevels stand for both optical pumping (by $\sigma^{\pm}$ and $\pi$ light) and spontaneous emission.

In this work we have analyzed theoretically and experimentally the influence of transverse magnetic fields $B_{\text{trans}}$ on amplitudes and widths of the EIA, in Rb atoms for different polarizations of the laser light. Hanle transmission curves were calculated and measured when the laser is locked to either $F_g=3\rightarrow F_e=4$ transition in $^{85}$Rb or to $F_g=2\rightarrow F_e=3$ transition in $^{87}$Rb. Effects of $B_{\text{trans}}$ are presented for linearly and for circularly polarized laser light. Also shown are the results for the laser light polarization which is close to linear and polarization close to circular, in order to separate potential influence of the polarization from the influence of the transverse magnetic field. We have analyzed effects of $B_{\text{trans}}$ for two possible directions of $\vec{B}_{\text{trans}}$ in a plane of the laser light polarization. In this paper, we present a systematic study on the dependence of EIA on both additional magnetic fields, and on the laser polarization.

## II. THEORETICAL MODEL

In this section we present the model used to calculate the transmission of a laser beam, resonant to the closed $F_g=2\rightarrow F_e=3$ transition of $^{87}$Rb or $F_g=3\rightarrow F_e=4$ transition of $^{85}$Rb. The atomic level schemes used in the calculations are presented in Fig. 1. Zeeman sublevels are coupled by the arbitrarily polarized laser field propagating along the $z$ axis, which is the direction of the $\vec{B}_{\text{scan}}$. Laser electric field is given by

$$\vec{E}(\vec{r}_0,t)=\vec{e}_x^{\,*}\cos(\omega_{(1)}t)E^*_{(1)0x}+\vec{e}_y^{\,*}\cos(\omega_{(1)}t+\varphi^{yx}_{(1)})E^*_{(1)0y}. \tag{1}$$

The laser elliptical polarization is characterized by ellipticity $\chi$, as given by

$$\tan\chi=\frac{E_{(1)0y}}{E_{(1)0x}}. \tag{2}$$

In our study we consider the two possible directions of $\vec{B}_{\text{trans}}$ (see Fig. 2). In Fig. 2 $\vec{B}_{\text{total}}$ and $\alpha$ are

$$\vec{B}_{\text{total}}=\vec{B}_{\text{scan}}+\vec{B}_{\text{trans}},$$

$$\alpha=\arctan\frac{B_{\text{total}}}{B_{\text{scan}}}. \tag{3}$$

Using quantization axis parallel to total magnetic field in the rotated coordinate system $\vec{B}_{\text{total}}$, elliptical polarization becomes

$$\vec{E}(\vec{r}_0,t)=\vec{e}_x\cos(\omega_{(1)}t)E_{(1)0x}+\vec{e}_y\cos(\omega_{(1)}t+\varphi^{yx}_{(1)})E_{(1)0y}+\vec{e}_z\cos(\omega_{(1)}t+\varphi^{zx}_{(1)})E_{(1)0z}, \tag{4}$$

where

$$E_{(1)0}=(E^{*2}_{(1)0x}+E^{*2}_{(1)0y})^{1/2}=(E^2_{(1)0x}+E^2_{(1)0y}+E^2_{(1)0z})^{1/2} \tag{5}$$

is the amplitude of the laser electric field. This choice of quantization axis means that Zeeman sublevels are coupled by $\sigma^+$, $\sigma^-$, and $\pi$ light, resulting, as shown in Fig. 1, in multiple $V$-atomic schemes.

Optical Bloch equations were solved for density matrix elements $\rho_{i,j}$ for the atomic system of magnetic sublevels of both the ground and of the excited states. Assuming pure radiative relaxation and the closed system, equations have the following form:

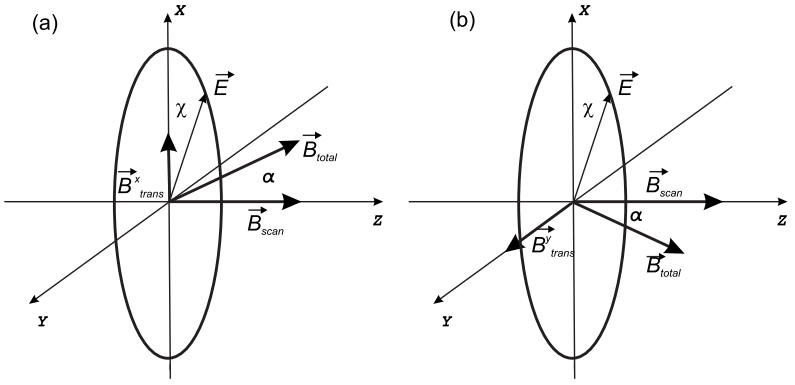


FIG. 2. Two directions of $\vec{B}_{\text{trans}}$ which were taken into consideration: (a) $\vec{B}^x_{\text{trans}}$, along the $x$ axis; (b) $\vec{B}^y_{\text{trans}}$, along the $y$ axis. The laser light propagates along the $z$ axis. Note that laser electric field $\vec{E}$ for linear polarization and major axis of polarization ellipse are always directed along the $x$ axis, but we change direction of $\vec{B}_{\text{trans}}$.

$$\dot{\varrho}_{e_ie_j} = \left(-\frac{2}{(2F_e+1)}\Gamma_L|\mathcal{G}_1|^2 + i(\omega_{e_j}-\omega_{e_i})\right)\varrho_{e_ie_j}$$
$$+ i\sum_{l=-F_g}^{F_g}\{\tilde{\varrho}_{e_ig_l}[\mu_{g_l,e_j,-1}(-\mathcal{G}_{2x}-ie^{i\varphi^{yx}_{(1)}}\mathcal{G}_{2y}) + \mu_{g_l,e_j,1}(\mathcal{G}_{2x}-ie^{i\varphi^{yx}_{(1)}}\mathcal{G}_{2y}) - \mu_{g_l,e_j,0}\sqrt{2}\mathcal{G}_{2z}e^{i\varphi^{zx}_{(1)}}]$$
$$+ [\mu_{e_i,g_l,-1}(\mathcal{G}_{2x}+ie^{-i\varphi^{yx}_{(1)}}\mathcal{G}_{2y}) + \mu_{e_i,g_l,1}(-\mathcal{G}_{2x}+ie^{-i\varphi^{yx}_{(1)}}\mathcal{G}_{2y}) + \mu_{g_l,e_j,0}\sqrt{2}\mathcal{G}_{2z}e^{-i\varphi^{zx}_{(1)}}]\tilde{\varrho}_{g_le_j}\} - \gamma\varrho_{e_ie_j},$$

$$\dot{\tilde{\varrho}}_{e_ig_j} = \left(-\frac{\Gamma_L}{(2F_e+1)}|\mathcal{G}_1|^2 + i(\omega_{(1)}+\omega_{g_j}-\omega_{e_i})\right)\tilde{\varrho}_{e_ig_j}$$
$$+ i(\sum_{l=-F_e}^{F_e}\{\varrho_{e_ie_l}[\mu_{e_l,g_j,-1}(-\mathcal{G}_{2x}-ie^{-i\varphi^{yx}_{(1)}}\mathcal{G}_{2y}) + \mu_{e_l,g_j,1}(\mathcal{G}_{2x}-ie^{-i\varphi^{yx}_{(1)}}\mathcal{G}_{2y}) - \mu_{e_l,g_j,0}\sqrt{2}\mathcal{G}_{2z}e^{-i\varphi^{zx}_{(1)}}]\}$$
$$+ \sum_{l=-F_g}^{F_g}\{[\mu_{e_i,g_l,-1}(\mathcal{G}_{2x}+ie^{-i\varphi^{yx}_{(1)}}\mathcal{G}_{2y}) + \mu_{e_i,g_l,1}(-\mathcal{G}_{2x}+ie^{-i\varphi^{yx}_{(1)}}\mathcal{G}_{2y}) + \mu_{e_i,g_l,0}\sqrt{2}\mathcal{G}_{2z}e^{-i\varphi^{zx}_{(1)}}]\varrho_{g_lg_j}\}) - \gamma\tilde{\varrho}_{e_ig_j},$$

$$\dot{\tilde{\varrho}}_{g_je_i} = \left[-\frac{\Gamma_L}{(2F_e+1)}|\mathcal{G}_1|^2 + i(-\omega_{(1)}+\omega_{e_i}-\omega_{g_j})\right]\tilde{\varrho}_{g_je_i}$$
$$+ i(\sum_{l=-F_g}^{F_g}\{\varrho_{g_jg_l}[\mu_{g_l,e_i,-1}(-\mathcal{G}_{2x}-ie^{i\varphi^{yx}_{(1)}}\mathcal{G}_{2y}) + \mu_{g_l,e_i,1}(\mathcal{G}_{2x}-ie^{i\varphi^{yx}_{(1)}}\mathcal{G}_{2y}) - \mu_{g_l,e_i,0}\sqrt{2}\mathcal{G}_{2z}e^{i\varphi^{zx}_{(1)}}]\}$$
$$+ \sum_{l=-F_e}^{F_e}\{[\mu_{g_j,e_l,-1}(\mathcal{G}_{2x}+ie^{i\varphi^{yx}_{(1)}}\mathcal{G}_{2y}) + \mu_{g_j,e_l,1}(-\mathcal{G}_{2x}+ie^{i\varphi^{yx}_{(1)}}\mathcal{G}_{2y}) + \mu_{g_j,e_l,0}\sqrt{2}\mathcal{G}_{2z}e^{i\varphi^{zx}_{(1)}}]\varrho_{e_le_i}\}) - \gamma\tilde{\varrho}_{g_je_i},$$

$$\dot{\varrho}_{g_ig_j} = (2\sum_{q=-1}^{1}\mu_{e_{i+q},g_i,q}\mu^*_{e_{j+q},g_j,q}\varrho_{e_{i+q}e_{j+q}}\Gamma_L + i(\omega_{g_j}-\omega_{g_i})\varrho_{g_ig_j})$$
$$+ i\sum_{l=-F_e}^{F_e}\{\tilde{\varrho}_{g_ie_l}[\mu_{e_l,g_j,-1}(-\mathcal{G}_{2x}-ie^{-i\varphi^{yx}_{(1)}}\mathcal{G}_{2y}) + \mu_{e_l,g_j,1}(\mathcal{G}_{2x}-ie^{-i\varphi^{yx}_{(1)}}\mathcal{G}_{2y}) - \mu_{e_l,g_j,0}\sqrt{2}\mathcal{G}_{2z}e^{-i\varphi^{zx}_{(1)}}]$$
$$+ [\mu_{g_i,e_l,-1}(\mathcal{G}_{2x}+ie^{i\varphi^{yx}_{(1)}}\mathcal{G}_{2y}) + \mu_{g_i,e_l,1}(-\mathcal{G}_{2x}+ie^{i\varphi^{yx}_{(1)}}\mathcal{G}_{2y}) + \mu_{g_i,e_l,0}\sqrt{2}\mathcal{G}_{2z}e^{i\varphi^{zx}_{(1)}}]\tilde{\varrho}_{e_lg_j}\} - \gamma\left(\varrho_{g_ig_j} - \frac{1}{(2F_g+1)}\delta_{ij}\right), \quad (6)$$

where $g$ and $e$ refer to the ground and the excited state hyperfine levels, respectively. Fast oscillations at laser frequency $\omega_{(1)}$ in Eq. (6) were eliminated by the usual substitution

$$\varrho_{e_ig_j} = \tilde{\varrho}_{e_ig_j}e^{-i\omega_{(1)}t}. \quad (7)$$

In Eq. (6), $\mu_{a,b,q}=e\langle a|\vec{u}_q\vec{r}|b\rangle$, where the symbols $a$ and $b$ indicate any ground or excited Zeeman sublevel given by the quantum number $m_{g(e)}$. $\mathcal{G}_1$ is the constant proportional to the reduced matrix element of the dipole operator between the ground and the excited states,

$$\mathcal{G}_1 \sim \langle n_eL_e\|\vec{r}\|n_gL_g\rangle \quad (8)$$

which is taken from [28]. The expression for $\mu$ then becomes

$$\mu_{m_e,m_g,q} = \mathcal{G}_1(-1)^{m_e}\begin{pmatrix} F_g & 1 & F_e \\ m_g & q & -m_e \end{pmatrix}_{3J}, \quad (9)$$

where $q=0,\pm1$. Amplitude of the laser electric field enters equations in quantities,

$$\mathcal{G}_{2i} = \frac{E_{(1)0i}}{2\sqrt{2}\hbar}, \quad i=x,y,z, \quad (10)$$

where $E_{(1)0i}$ are components of the laser electric field vector $\vec{E}$ in a rotated coordinate system. For the case of $\vec{B}_{\text{trans}}=\vec{B}^x_{\text{trans}}$ ($\vec{B}_{\text{trans}}$ directed along $\pm\vec{e}_x$) rotation is performed around $\vec{e}_y$, and parameters were changed accordingly to

$$E_{(1)0x} = \cos\alpha E^*_{(1)0x},$$

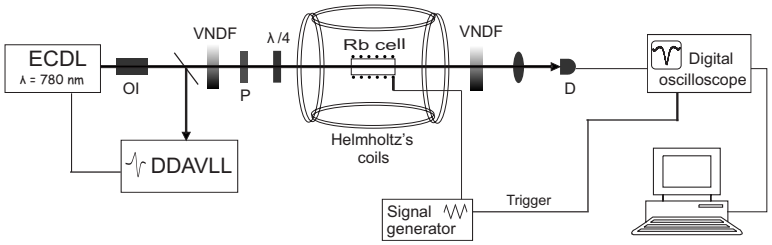


FIG. 3. Experimental setup. External cavity diode laser (ECDL), optical insulator (OI), Doppler-free dichroic atomic vapor laser lock (DDAVLL), variable neutral density filter (VNDF), polarizer ($P$), detector ($D$).

$$E_{(1)0y} = E^*_{(1)0y},$$

$$E_{(1)0z} = \pm \sin \alpha E^*_{(1)0x},$$

$$\varphi^{yx}_{(1)} = \varphi^{yx*}_{(1)},$$

$$\varphi^{zx}_{(1)} = 0. \tag{11}$$

If $\vec{B}_{\text{trans}} = \vec{B}^y_{\text{trans}}$ ($\vec{B}_{\text{trans}}$ directed along $\pm\vec{e}_y$), rotation is performed around $\vec{e}_x$ and parameters were changed as

$$E_{(1)0x} = E^*_{(1)0x},$$

$$E_{(1)0y} = \cos \alpha E^*_{(1)0y},$$

$$E_{(1)0z} = \mp \sin \alpha E^*_{(1)0y},$$

$$\varphi^{yx}_{(1)} = \varphi^{yx*}_{(1)},$$

$$\varphi^{zx}_{(1)} = \varphi^{yx*}_{(1)}. \tag{12}$$

Here $\varphi^{yx}_{(1)}$ ($\varphi^{zx}_{(1)}$) stand for phase differences between $y$ and $x$ ($z$ and $x$) electric field components.

In Eq. (6) $E_{g(e)} = \omega_{g(e)}\hbar$ are energies describing Zeeman splitting due to applied magnetic field $\vec{B}_{\text{total}}$ of the ground and excited levels with quantum numbers $m_{g(e)}$ and were calculated as

$$E_{g(e)} = \mu_B g_{F_{g(e)}} m_{g(e)} B_{\text{total}}. \tag{13}$$

Here $\mu_B$ is the Bohr magneton and $g_{F_{g(e)}}$ is the Landé gyromagnetic factor for two hyperfine levels. Laser detuning, which is the difference between laser frequency and the resonance frequency is given by

$$\Delta_D = \omega_{(1)} - (\omega_{e_0} - \omega_{g_0}). \tag{14}$$

In Eq. (6) $\frac{2}{2F_e+1}\Gamma_L|\mathcal{G}_1|^2 = \Gamma$, where $\Gamma$ is the total spontaneous emission rate of any excited state ($2\pi \times 5.89$ for $^{85}$Rb, and $2\pi \times 6.06$ for $^{87}$Rb). The ground-state relaxation rate is given by $\gamma$. In the absence of relaxation mechanisms in the vacuum Rb vacuum cell (we assume that collisions do not play any role in the coherence lifetime because of low atomic density), $\gamma$ is determined by the atom transit time through the laser beam. It describes the rate at which atoms enter and leave the laser beam. Under these assumptions we have calculated $\gamma$ from $\gamma = v_{mp}/r$ [29], where $v_{mp} = \sqrt{2k_BT/M}$ is the most probable velocity of the atoms (equal $\sim$240 m/s for Rb atoms at room temperature) and $r = 2.45$ mm is the radius of the laser beam.

The system of equations given in (6) was solved assuming a steady state of an atomic system, an approximation which is correct for cold atoms. Our experimental results can be compared to the steady state solution of Eq. (6) since the estimated atom transit time through the laser beam is longer than calculated time required for atoms to reach a steady state when suddenly illuminated by light tuned to a closed transition [30].

As a spectroscopic signal we consider the total excited-state population

$$\Pi_e = \sum \varrho_{e_i e_i} \tag{15}$$

as a function of the magnetic field amplitude $B_{\text{scan}}$. Since all atoms in the excited state decay at the same rate, this number is proportional to the light absorption coefficient in optically thin media. Theoretical results shown below as a laser transmission spectroscopic signal are in fact $(1-\Pi_e)$. The dependence of this quantity on $B_{\text{scan}}$ is the Hanle transmission curve and we denote it by $T$.

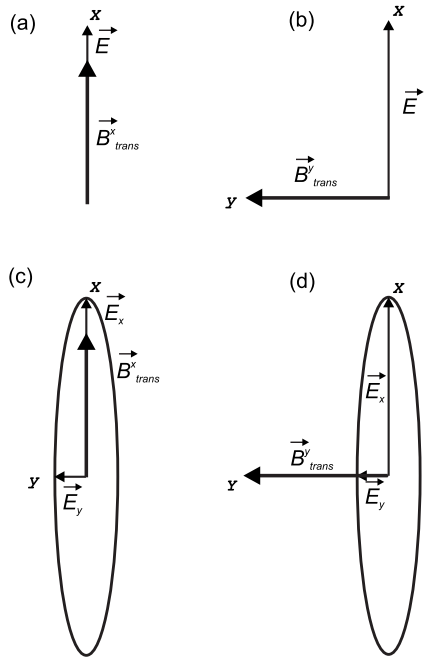


FIG. 4. Mutual orientations of $\vec{B}_{\text{trans}}$ and $\vec{E}$ considered in our analysis: (a) and (b) linear polarization; (c) and (d) elliptical polarization $\chi = 10°$.

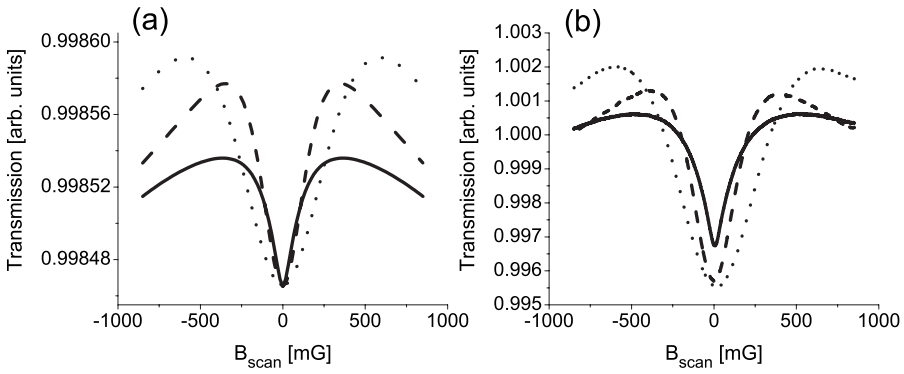


FIG. 5. Calculated (a) and measured (b) Hanle EIA resonances for linearly polarized laser light, when $\vec{B}_{\text{trans}} \| \vec{E}$ for $^{87}$Rb. The laser intensity is $I=0.6$ mW/cm$^2$; solid curves, $B^x_{\text{trans}}=0$; dashed curves, $B^x_{\text{trans}}=200$ mG; and dotted curves, $B^x_{\text{trans}}=460$ mG.

The Doppler effect was taken into account in calculations of the total light transmission by averaging transmission curves, calculated for a single atomic velocity, over velocities in the range $(-700, 700)$ m/s according to

$$T = \sum T(v_i) w(v_i), \tag{16}$$

where $w(v_i)$ are the weights of the Maxwell-Boltzmann distribution $f(v)$. We calculated them as

$$w(v_i) = \int_{v_{i-1}+v_i/2}^{v_i+v_{i+1}/2} f(v) dv. \tag{17}$$

$T(v_i)$ is the transmission curve for the range of the scanning field $B_{\text{scan}}$ from −0.85 to 0.85 G, for a particular atomic velocity $v_i$, i.e., for the laser frequency detuning $\Delta_D$ (1.28 MHz per atomic velocity of 1 m/s). As indicated in [31], due to different rates at which Hanle profiles change with atomic velocities at low and at high atomic velocities, partition of $f(v)$ was not uniform. Instead, our partition is denser at lower velocities, which ensure a good approximation to the convo-

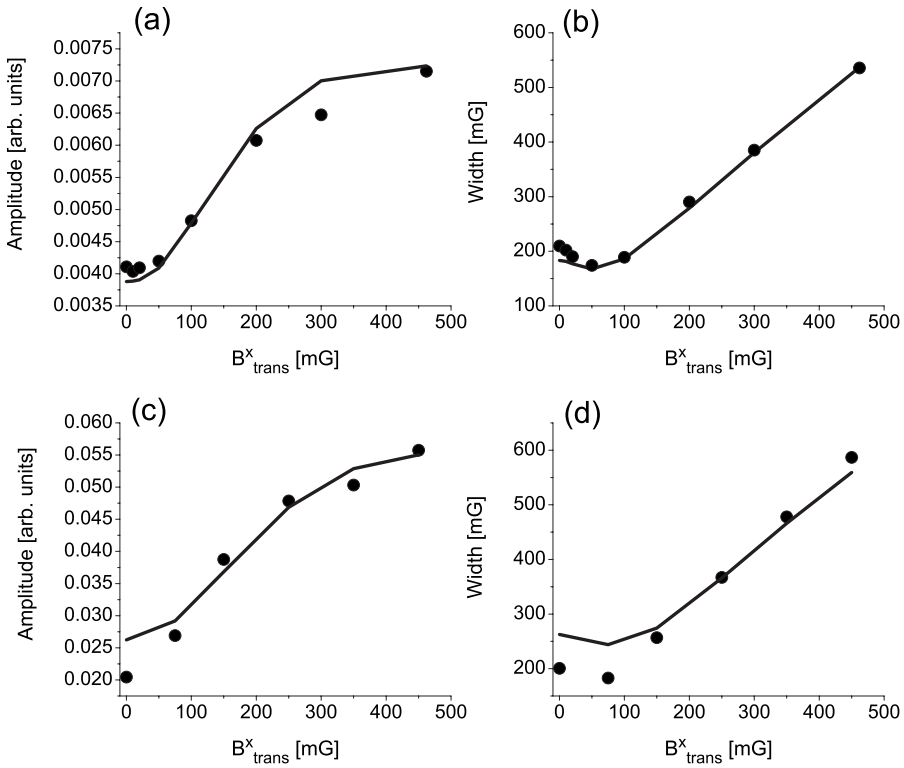


FIG. 6. Calculated (curves) and measured (points) amplitudes [(a) and (c)] and widths [(b) and (d)], of the EIA for $^{87}$Rb [(a) and (b)] and for $^{85}$Rb [(c) and (d)]. $\vec{B}_{\text{trans}} \| \vec{E}$. The laser intensities were $I=0.6$ mW/cm$^2$ [(a) and (b)] and $I=1$ mW/cm$^2$ [(c) and (d)]. Theoretical results for amplitudes were scaled from amplitudes in Fig. 5 by the constant number.

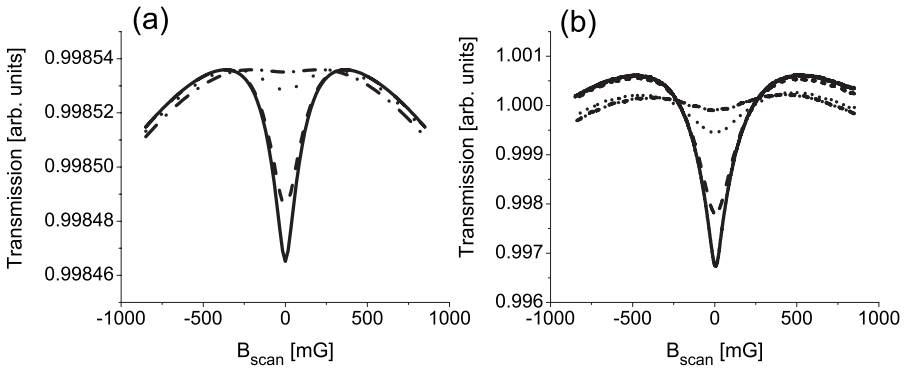


FIG. 7. Calculated (a) and measured (b) Hanle EIA resonances for linearly polarized laser light, for $^{87}$Rb. $\vec{B}_{\text{trans}} \perp \vec{E}$. Solid curves, $B^{y}_{\text{trans}}=0$; dashed curves, $B^{y}_{\text{trans}}=50$ mG; dotted curves, $B^{y}_{\text{trans}}=200$ mG; and dashed-dotted curves, $B^{y}_{\text{trans}}=300$ mG. The laser intensity is $I=0.6$ mW/cm$^2$.

lution integral, and also saves computation time.

## III. EXPERIMENTAL SETUP

The experiment is schematically shown in Fig. 3. An extended cavity diode laser is frequency locked to either the $F_g=2\rightarrow F_e=3$ transition of $^{87}$Rb or $F_g=3\rightarrow F_e=4$ transition of $^{85}$Rb, by a Doppler-free dichroic atomic vapor laser lock (DDAVLL) technique [32]. Both transitions are closed transitions in $D2$ lines, and both start from a higher ground-state hyperfine level. Of the three allowed transitions to excited state hyperfine levels, unresolved due to the Doppler broadening, the one that is used for laser locking is the strongest and determines the resonance sign. The laser light intensity and polarization are set by a combination of half-wave and quarter-wave plates, and a linear polarizer. The laser light passes through the Rb cell before its intensity is detected by the photodiode. The Rb cell is placed inside a solenoid which generates scanning magnetic field ($B_{\text{scan}}$) in the range from −0.85 to 0.85 G. We used two cells, 8-cm-long cell with natural abundance of Rb isotopes for experiments with $^{85}$Rb, and 1.5-cm-long cell enriched with $^{87}$Rb for experiments with $^{87}$Rb. As shown below, there are no noticeable differences between the results obtained with two Rb isotopes in two different cells. This showed that different optical paths and laser absorption, polarization rotation, and noncompensated stray magnetic fields away from the center of the Helmholtz cage had a negligible role in our measurements of EIA. The Rb cell is in the center of three pairs of large, mutually orthogonal Helmholtz coils. Separate current sources for the Helmholtz coils allow compensation of the stray magnetic field resulting in a residual magnetic field of $\approx 1$ mG as measured by a Gauss meter. One of the Helmholtz coils was also used to generate controllable magnetic fields $\vec{B}_{\text{trans}}$, transverse to the scanning $\vec{B}_{\text{scan}}$ magnetic field. Before the photodiode, the laser beam is attenuated by variable neutral density filter to about the same dc level to avoid saturation and diode's different responses at different light levels. The diode signal proportional to the laser light transmitted through the Rb cell was averaged using a digital oscilloscope.

## IV. COMPARISON BETWEEN THEORETICAL AND EXPERIMENTAL RESULTS

We now compare theoretical and experimental results obtained in order to understand the behavior of the EIA in configuration with crossed magnetic fields, when laser light

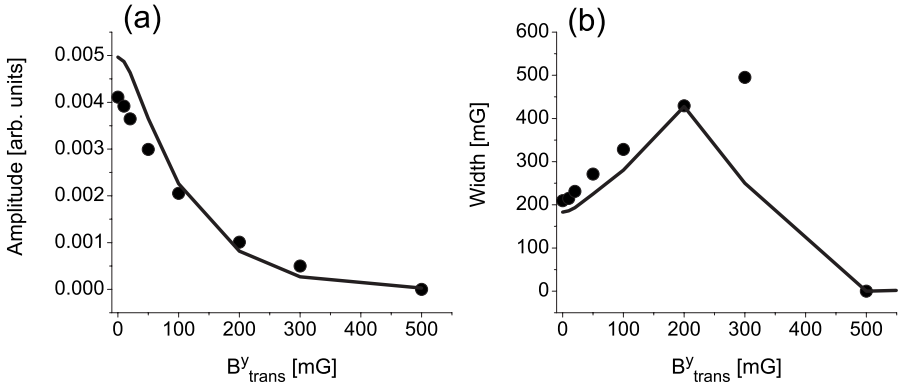


FIG. 8. Calculated (curves) and measured (points) amplitudes (a) and widths (b), of the EIA for $^{87}$Rb. The laser polarization is linear, $\vec{B}_{\text{trans}} \perp \vec{E}$, and intensity is $I=0.6$ mW/cm$^2$. Theoretical results for amplitudes were scaled from amplitudes in Fig. 7 by the constant number.

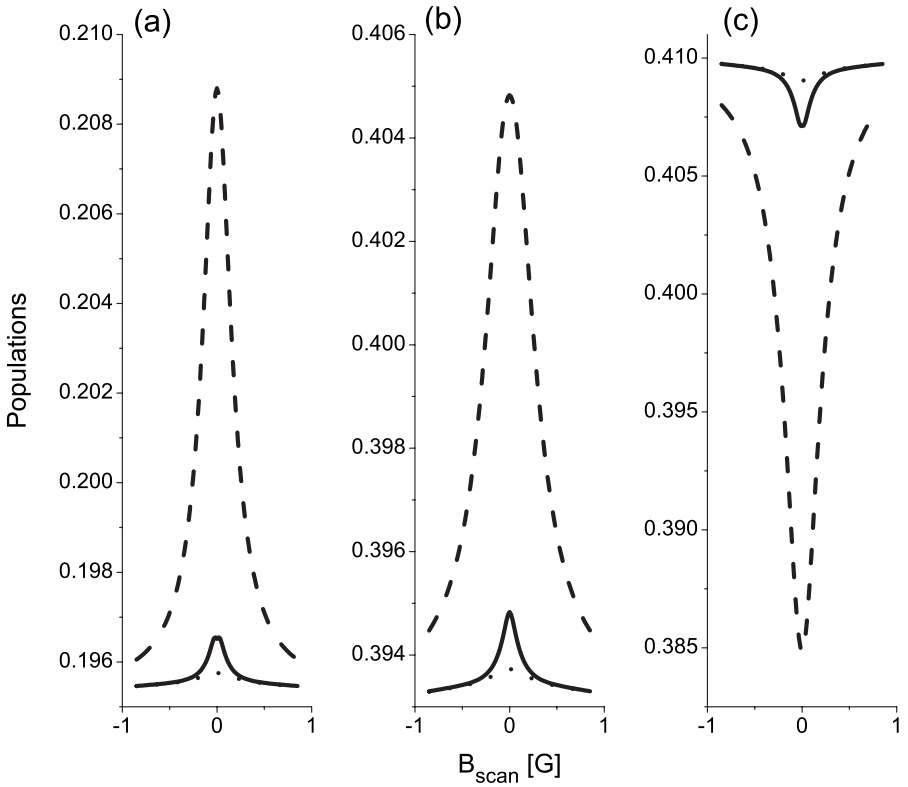


FIG. 9. Calculated populations of ground-state sublevels for $^{87}$Rb. Laser light polarization is linear and intensity is $I=0.6$ mW/cm$^2$; population of (a) $m_g=0$, (b) sum of $m_g=1$ and $m_g=-1$, (c) sum of $m_g=2$ and $m_g=-2$; solid curves, $B_{\text{trans}}=0$ mG; dashed curves, $B^x_{\text{trans}}=200$ mG; and dotted curves, $B^y_{\text{trans}}=200$ mG.

has different polarizations. We analyzed closed transitions $F_g=2\rightarrow F_e=3$ in $^{87}$Rb or $F_g=3\rightarrow F_e=4$ in $^{85}$Rb of the $D2$ line. The work has been done for the laser light with different polarizations, linear, elliptical, and circular. The presentation of the results is as follows. We divide our results into three separate sections: Sec. IV A for linear; Sec. IV B for near linear; and Sec. IV C for circular and close-to-circular laser polarization. We have analyzed two cases, i.e., two possible directions of $\vec{B}_{\text{trans}}$ in plane of the laser light polarization (see Fig. 2). We present our results for EIA amplitudes and widths as a function of transverse magnetic fields for $B_{\text{trans}}$ changing from zero in only one direction. Experimental and theoretical results for $\vec{B}_{\text{trans}}$ in opposite directions are identical to the presented results. Amplitudes were evaluated, such as the difference between transmission minimum at $B_{\text{scan}}=0$ and the value of the fit of the Hanle profile, in the absence of EIA, also at $B_{\text{scan}}=0$. EIA widths are full width at half-maximum of the Hanle resonance. Calculated and measured results for widths can be directly compared, because our theoretical model gives widths in units of $B_{\text{scan}}$. Theoretical results for amplitudes were scaled with a constant number in

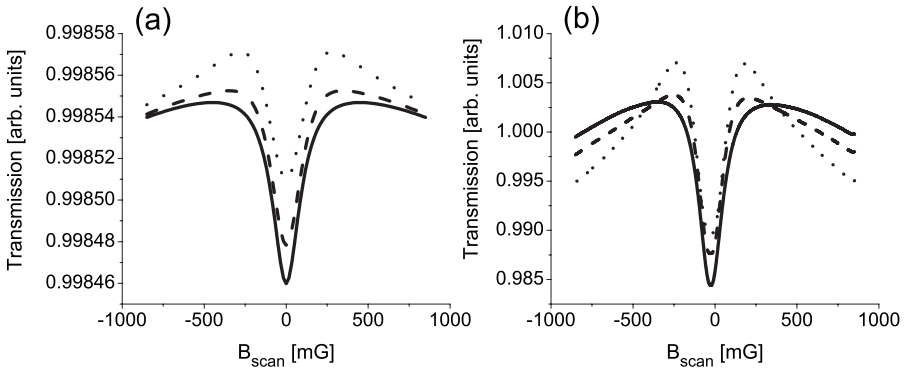


FIG. 10. Calculated (a) and measured (b) Hanle EIA resonances for elliptically polarized laser light, $\chi=10°$, when $\vec{B}_{\text{trans}}\|\vec{e}_x$ (i.e., parallel to the major axis of polarization ellipse) for $^{85}$Rb. The laser intensity is $I=0.6$ mW/cm$^2$; solid curves, $B^x_{\text{trans}}=0$; dashed curves, $B^x_{\text{trans}}=50$ mG; and dotted curves, $B^x_{\text{trans}}=100$ mG.

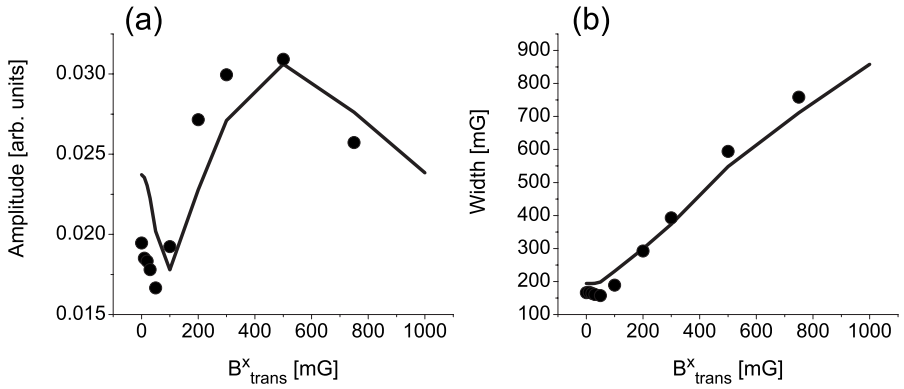


FIG. 11. Calculated (curves) and measured (points) amplitudes (a) and widths (b), of the EIA for $^{85}$Rb. The laser ellipticity $\chi=10°$, $\vec{B}_{\text{trans}}\|\vec{e}_x$, and intensity is $I=0.6$ mW/cm$^2$. Theoretical results for amplitudes were scaled from amplitudes in Fig. 10 by the constant number.

order to present them together with the experimental results.

### A. EIA excitation with linearly polarized laser light

Effects of homogeneous magnetic field, parallel to the laser electrical vector, $\vec{B}_{\text{trans}}\|\vec{E}$ [Fig. 4(a)] on the Hanle EIA wave forms, EIA amplitudes and widths, for $^{87}$Rb, are shown in Figs. 5 and 6. Theoretical and experimental Hanle curves for three values of $B^x_{\text{trans}}$, presented in Figs. 5(a) and 5(b), show very similar wave forms for both central regions (EIA resonance) and adjacent regions (single photon absorption). As seen from these results in Fig. 6, the EIA amplitude increases with $B^x_{\text{trans}}$, while EIA width gets wider only when values of $B^x_{\text{trans}}$ are above 100 mG. When the transverse magnetic field $\vec{B}^x_{\text{trans}}$ is parallel to the laser polarization and $B_{\text{scan}}=0$, quantization axis is taken along the same direction. This configuration enables optical pumping in the $m_g=0$ sublevel since it is the sublevel most coupled to the laser light. This increases absorption at $B_{\text{scan}}=0$. Therefore, the role of the transverse magnetic field is such that it enhances the alignment at $B_{\text{scan}}=0$, and thus increase of $B_{\text{scan}}$ destroys the alignment more slowly. While amplitudes and widths for $^{87}$Rb were calculated and measured at the laser intensity of 0.6 mW/cm$^2$ [Figs. 6(a) and 6(b)], results shown for $^{85}$Rb [Figs. 6(c) and 6(d)] are for the input laser intensity of 1 mW/cm$^2$. Similarity between results with two different Rb isotopes is evident from Fig. 6. In the following figures we will show either results for $^{85}$Rb or $^{87}$Rb.

When magnetic field $\vec{B}^y_{\text{trans}}$, orthogonal to the laser polarization [see Fig. 4(b)] is applied, Hanle EIA for linearly polarized laser light behaves as we show in Figs. 7 and 8. Relatively good agreement between Hanle profiles at different $B^y_{\text{trans}}$ obtained in the experiment and calculated is evident in Figs. 7(a) and 7(b). One can see from Figs. 8(a) and 8(b) that the effect of $B^y_{\text{trans}}$ on EIA is different from the effect produced by $B^x_{\text{trans}}$. Coherences at $B_{\text{scan}}=0$ are destroyed when $B^y_{\text{trans}}$ reaches 400–500 mG. Changes of EIA widths, as shown in Fig. 8(b), are also quite different compared with the behavior of EIA when additional magnetic field is $B^x_{\text{trans}}$. According to the results in Fig. 8, at high transverse magnetic fields, experimental EIA widths increase until EIA vanishes, while theory predicts the range of $B^y_{\text{trans}}$ when EIA narrows before it disappears. Transverse magnetic field, perpendicular to the laser polarization, acts on the induced alignment at $B_{\text{scan}}=0$ in a similar manner as $B_{\text{scan}}\neq 0$ with $B_{\text{trans}}=0$, it transfers population away from magnetic sublevels strongly coupled by the laser light. This is evident from calculations of Zeeman sublevels populations when $B_{\text{trans}}$ is present (Fig.

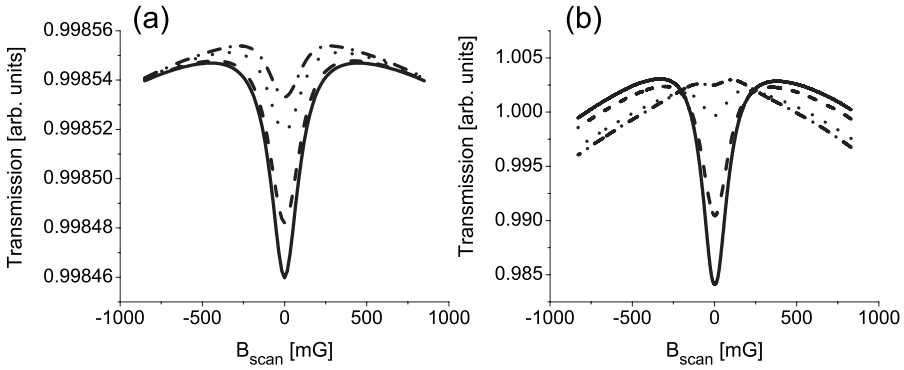


FIG. 12. Calculated (a) and measured (b) Hanle EIA resonances for elliptically polarized laser light, for $^{85}$Rb. $\vec{B}_{\text{trans}}\|\vec{e}_y$ is parallel to the minor axis of the polarization ellipse. The laser ellipticity is $\chi=10°$, and the intensity is $I=0.6$ mW/cm$^2$. Solid curves, $B^y_{\text{trans}}=0$; dashed curves, $B^y_{\text{trans}}=50$ mG; dotted curves, $B^y_{\text{trans}}=100$ mG; and dashed-dotted curves, $B^y_{\text{trans}}=120$ mG.

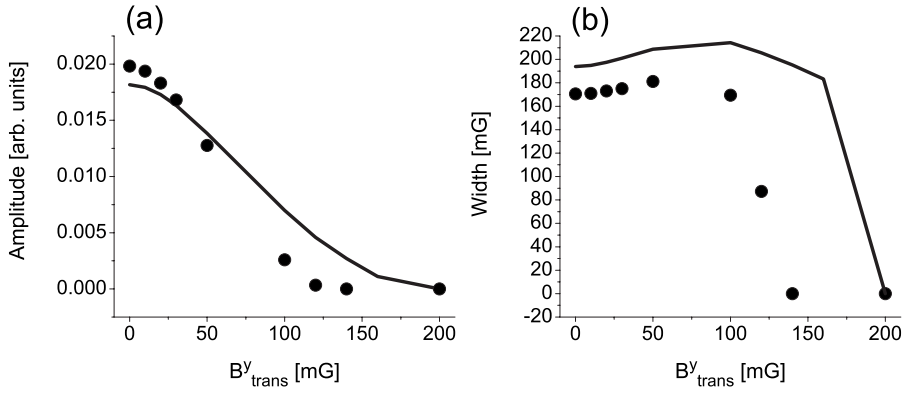


FIG. 13. Calculated (curves) and measured (points) amplitudes (a) and widths (b) of the EIA for $^{85}$Rb. The laser polarization is elliptical $\chi=10°$, $\vec{B}_{\text{trans}}\|\vec{e}_y$, and intensity is $I=0.6$ mW/cm$^2$. Theoretical results for amplitudes were scaled from amplitudes in Fig. 12 by the constant number.

9). Theoretical results for the Hanle EIA are in fact a combined contribution of atomic populations of different Zeeman ground sublevels. Populations of Zeeman sublevels of the ground-state hyperfine level $F_g=2$ as a function of $B_{\text{scan}}$ are calculated for different values and directions of $\vec{B}_{\text{trans}}$. We see that additional magnetic field in the $x$ direction, $B^x_{\text{trans}}=200$ mG, enhances the EIA by moving populations to inner magnetic sublevels, i.e., by changing the atomic orientation. The same value of magnetic field but directed along the $y$ axis, $B^y_{\text{trans}}$, eliminates EIA altogether.

### B. EIA excitation with elliptically ($\chi=10°$) polarized laser light

Next, we compare calculated and measured results, when in the presence of $B_{\text{trans}}$ the laser polarization has small deviation from linear. The ellipticity angle $\chi$ is 10°, or $E_{(1)0x}/E_{(1)0y}=5.67$. As for the linearly polarized light, we first present results when $\vec{B}_{\text{trans}}\|\vec{e}_x$ [see Fig. 4(c)]. The experimental results are compared with those calculated in Figs. 10 and 11. Here (Fig. 10) we show Hanle EIA resonances for $^{85}$Rb, comparing calculated (a) and measured (b) results, for different transverse magnetic fields. Indeed, according to these wave forms, and according to the results for EIA amplitudes and widths in Fig. 11, such change of ellipticity matters. Both calculated and experimental results, for both Rb isotopes, show EIA amplitudes going through a minimum at ~100 mG.

Results obtained when the laser light is elliptical (ellipticity $\chi=10°$), and $\vec{B}_{\text{trans}}$ is parallel to the minor axis of the ellipse [see Fig. 4(d)] show constant lowering of the EIA amplitude as a function of the $B^y_{\text{trans}}$. As for the EIA width, EIA gets narrower after some $B^y_{\text{trans}}$, before it vanishes. Results are presented in Figs. 12 and 13. Therefore, for both linearly and weakly elliptically polarized light, additional magnetic field $B^y_{\text{trans}}$, destroys the EIA. Although EIA amplitudes and widths vary similarly with $B^y_{\text{trans}}$ for linearly and weakly polarized light, there are some differences. $B^y_{\text{trans}}$ required to eliminate EIA is smaller for elliptically than for linearly polarized light (see Figs. 8 and 13). As both theoretical and experimental results show, the EIA width first increases with $B^y_{\text{trans}}$, and then slowly decreases with an increase of $B^y_{\text{trans}}$. Maximum of this curve is at lower $B^y_{\text{trans}}$ for elliptically polarized light.

### C. Atomic excitation with circular and close-to-circular polarized laser light

For a highly elliptical laser light, $\chi\geq 35°$, two orientations of $\vec{B}_{\text{trans}}$ [see Fig. 14(a)], parallel to the major or minor axis of ellipse, produce very similar results. In Fig. 15 we present the results for $\chi=35°$ ($E_{(1)0x}/E_{(1)0y}=1.42$). Figures 15(a) and

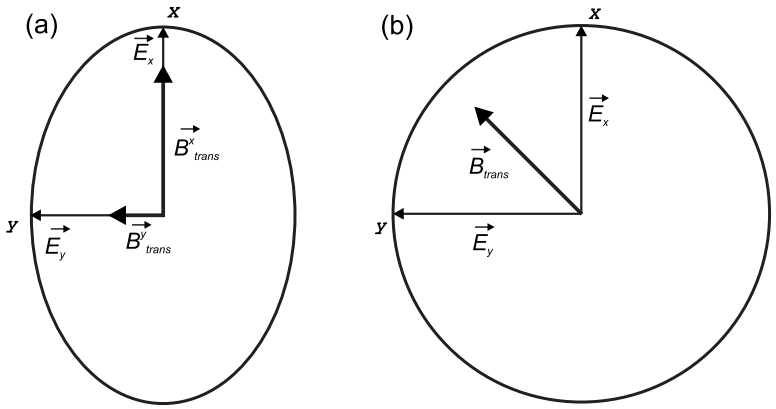


FIG. 14. Mutual orientations of $\vec{B}_{\text{trans}}$ and $\vec{E}$ considered in our analysis: (a) elliptical polarization $\chi=35°$ and (b) circular polarization.

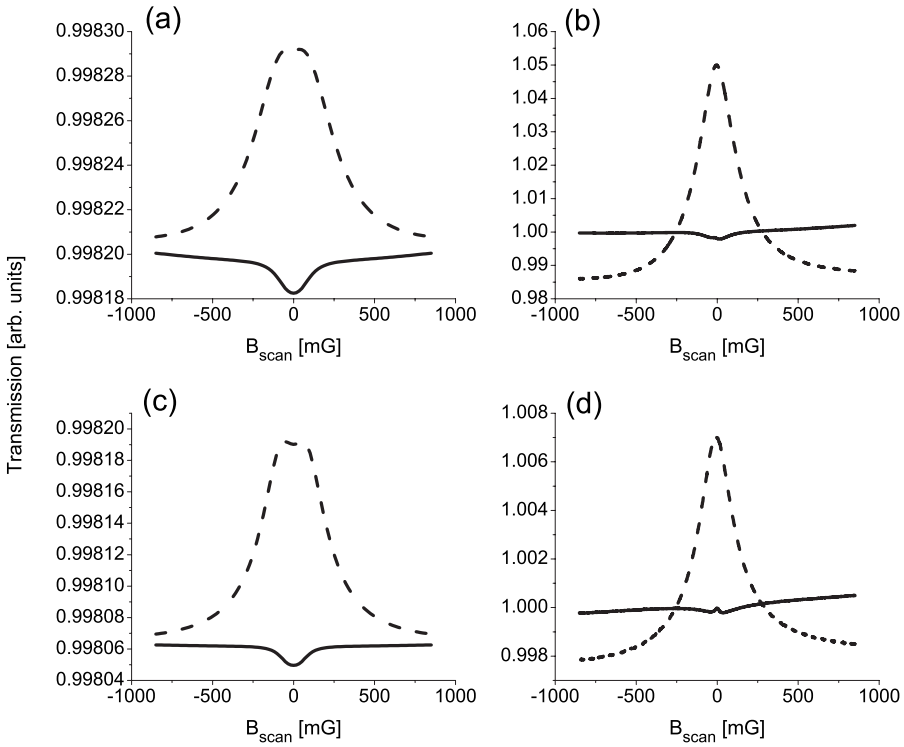


FIG. 15. Calculated [(a) and (c)] and measured [(b) and (d)] Hanle transmission data for elliptically polarized laser light, $\chi=35°$. Laser intensity is $I=0.6$ mW/cm$^2$. Results are for $^{85}$Rb and $\vec{B}_{\text{trans}} \| \vec{e}_x$ [(a) and (b)], and for $^{87}$Rb and $\vec{B}_{\text{trans}} \| \vec{e}_y$ [(c) and (d)]. Solid curves, $B^x_{\text{trans}}=0$ mG; dashed curves, $B^x_{\text{trans}}=100$ mG.

15(b) are for $\vec{B}_{\text{trans}}$ parallel to the major axis of the ellipse, and Figs. 15(c) and 15(d) are for $\vec{B}_{\text{trans}}$ parallel to the minor axis of the ellipse. Calculated and measured results give qualitatively the same behavior of the Hanle resonance with transverse magnetic fields. As we show theoretically and experimentally, for laser ellipticity this high, $B_{\text{trans}}$ has a strong influence on Hanle resonance and on the entire Hanle profile as well. For $B^x_{\text{trans}}<10$ mG and laser intensity considered

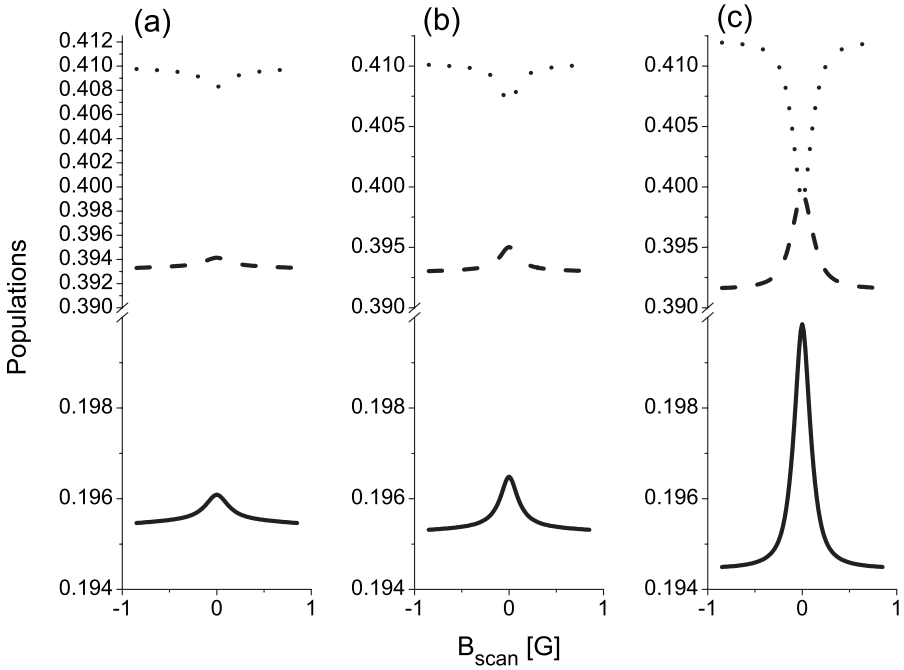


FIG. 16. Calculated populations of ground sublevels for $^{87}$Rb. $B^y_{\text{trans}}=100$ mG and intensity is $I=0.6$ mW/cm$^2$; (a) $\chi=0°$, (b) $\chi=10°$, (c) $\chi=35°$; solid curves, population of $m_g=0$; dashed curves, sum of $m_g=1$ and $m_g=-1$; and dotted curves, sum of $m_g=2$ and $m_g=-2$.

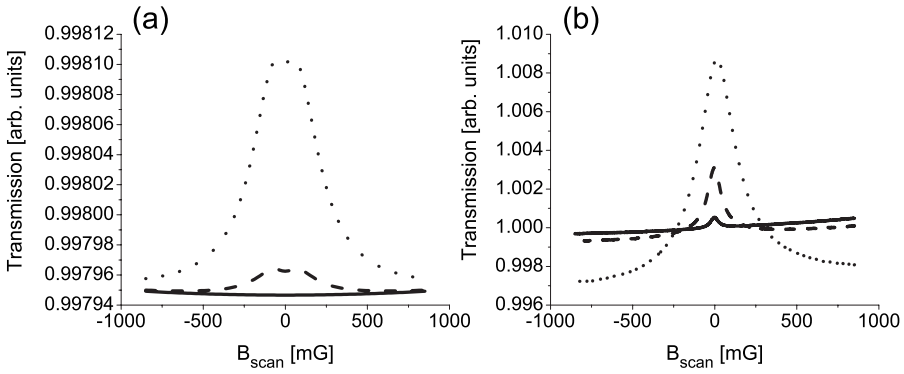


FIG. 17. Calculated (a) and measured (b) Hanle transmission data for circularly polarized laser light, for $^{87}$Rb and for the laser intensity of $I=0.6$ mW/cm$^2$; solid curves, $B_{\text{trans}}=0$ mG; dashed curves, $B_{\text{trans}}=30$ mG; and dotted curves, $B_{\text{trans}}=100$ mG.

here ($I=0.6$ mW/cm$^2$), a small EIA is observed. Increase of $B_{\text{trans}}$ leads to change of sign of the resonance and transmission peak dominates the Hanle transmission curve. Experimental result from Fig. 15(d) (solid curve) shows that $B_{\text{trans}}$ was not well compensated since the Hanle transmission profile has small EIT. This indicates the importance of control of stray magnetic field in experiments with EIA for laser ellipticity this high.

Like our results for the EIA, the results for CPT for highly elliptical light also show that the sign of the resonance depends if transverse (or stray) magnetic field is present or not [23]. It was shown [23] that if the Cs cell was not well shielded from laboratory magnetic field, CPT fluorescence dip switches to fluorescence gain.

It is evident from our results that for intensity considered here ($I=0.6$ mW/cm$^2$), EIA disappears with increase of $B^y_{\text{trans}}$. We have already discussed (in Sec. IV A) that it takes smaller $B^y_{\text{trans}}$ to destroy elliptical EIA than linear EIA. Differences produced on the EIA by $B^y_{\text{trans}}$ depending if the laser light is linear or elliptical are evident from populations of Zeeman sublevels calculated for three different ellipticities as a function of $B_{\text{scan}}$ (see Fig. 16). Figure 16 presents rapid variations of calculated magnetic sublevel populations in the presence of $B^y_{\text{trans}}=100$ mG when ellipticity increases. Note that dashed and dotted curves are, respectively, the sums of $m_g=\pm 1$ and $m_g=\pm 2$ populations. Dependence of the population of edge sublevels on $B_{\text{scan}}$ is different (has opposite sign) than dependence of population of inner Zeeman sublevels. While a sum of populations of edge sublevels ($m_g=\pm 2$) shows EIA, inner sublevels ($m_g=0$ and $m_g=\pm 1$) show EIT regardless of the ellipticity. It is evident from Figs. 16(a)–16(c) that light of higher ellipticity pumps more atoms into inner magnetic sublevels which for $\chi=35°$ leads to inversion of sign of the resonance. As the result, Hanle transmission profile shows EIT.

When the laser light is circularly polarized, and $B_{\text{trans}}=0$, no $V$ schemes can be formed between Zeeman sublevels of the ground and excited hyperfine levels. This light only pumps atoms into Zeeman sublevels of the edge $m_g$, creating a magnetic momentum directed along the $\vec{B}_{\text{scan}}$. Thus, Hanle transmission obtained by scanning $B_{\text{scan}}$ should show no resonances. This indeed is shown theoretically in Fig. 17(a), by the solid curve. Increase of the $B_{\text{trans}}$, which is in the plane of the laser light polarization [Fig. 14(b)], redistributes the atomic population, which causes an increase of the laser transmission at $B_{\text{scan}}=0$. Uncompensated magnetic fields in the experiment (measured to be around $\sim 1$ mG) cause small transmission gain as given by the solid line in Fig. 17(b). Induced transmission gain becomes higher as $B_{\text{trans}}$ becomes large, both its amplitude and width increasing with $B_{\text{trans}}$.

## V. CONCLUSION

This work presents, through calculated and measured results, strong variations of Hanle EIA when, in the presence of transverse magnetic fields, laser polarization takes different ellipticity. The investigations were carried on the $D2$ line of Rb, for the closed $F_g \rightarrow F_e=F_g+1$ atomic system. For linear polarization, when the laser electric vector is parallel to transverse magnetic field, enhancement of the EIA is observed. Increase of transverse magnetic field orthogonal to the laser electric vector weakens the EIA (and even diminishes it). Changing the laser polarization, from linear to near linear, does not change significantly qualitative and quantitative behavior of the EIA in the presence of $B_{\text{trans}}$. For laser light highly elliptically polarized, we have shown that EIA, as it was observed previously for CPT, is extremely sensitive to small transverse magnetic fields (and changes sign when these fields are higher). When the laser light is circularly polarized, both theory and experiment also show strong influence of very small stray magnetic fields on a Hanle profile. A nonzero transverse magnetic field induces coherences between Zeeman sublevels and Hanle transmission profile shows transmission peak for circularly polarized laser light. Theory and experiment agree well on shapes of Hanle profiles and on the dependence of EIA amplitudes and widths on transverse magnetic fields for the entire range which we considered in our analysis. Comprehensive studies presented here of effects of stray magnetic fields, transverse to the scanning magnetic field, and on the laser polarization on the EIA, emphasizes importance of good shielding from laboratory magnetic fields and careful verification of a degree of laser light polarization.

This work was supported by the Ministry of Science and Environmental Protection of the Republic of Serbia Grant No. 141003.

[1] G. Alzetta, L. Moi, and G. Orriols, Nuovo Cimento Soc. Ital. Fis., B **52B**, 209 (1979).
[2] E. Arimondo and G. Orriols, Lett. Nuovo Cimento Soc. Ital. Fis. **17**, 333 (1976).
[3] A. Kuhn, S. Steuerwald, and K. Bergmann, Eur. Phys. J. D **1**, 57 (1998).
[4] A. M. Akulshin, S. Barreiro, and A. Lezama, Phys. Rev. A **57**, 2996 (1998).
[5] A. M. Akulshin, S. Barreiro, and A. Lezama, Phys. Rev. Lett. **83**, 4277 (1999).
[6] A. Lezama, S. Barreiro, A. Lipsich, and A. M. Akulshin, Phys. Rev. A **61**, 013801 (1999).
[7] H. Failache, P. Valente, G. Ban, V. Lorent, and A. Lezama, Phys. Rev. A **67**, 043810 (2003).
[8] E. Arimondo, Prog. Opt. **35**, 257 (1996).
[9] O. A. Kocharovskaya and Y. I. Khanin, JETP Lett. **48**, 630 (1988).
[10] S. E. Harris, Phys. Rev. Lett. **62**, 1033 (1989).
[11] S. I. Kanorsky, A. Weis, J. Wurster, and T. W. Hansch, Phys. Rev. A **47**, 1220 (1993).
[12] C. Goren, A. D. Wilson-Gordon, M. Rosenbluh, and H. Friedmann, Phys. Rev. A **67**, 033807 (2003).
[13] A. V. Taichenachev, A. M. Tumaikin, and V. I. Yudin, Phys. Rev. A **61**, 011802(R) (1999).
[14] C. H. van der Wal, M. D. Eisaman, A. Andr, R. L. Walsworth, D. F. Phillips, A. S. Zibrov, and M. D. Lukin, Science **301**, 196 (2003).
[15] A. M. C. Dawes, L. Illing, S. M. Clark, and D. J. Gauthier, Science **308**, 672 (2005).
[16] I. Novikova, A. V. Gorshkov, D. F. Phillips, A. S. Sorensen, M. D. Lukin, and R. L. Walsworth, Phys. Rev. Lett. **98**, 243602 (2007).
[17] L. J. Wang, A. Kuzmich, and A. Dogariu, Nature (London) **406**, 277 (2000).
[18] A. M. Akulshin, A. Cimmino, A. I. Sidorov, P. Hannaford, and G. I. Opat, Phys. Rev. A **67**, 011801(R) (2003).
[19] A. Lezama, A. M. Akulshin, A. I. Sidorov, and P. Hannaford, Phys. Rev. A **73**, 033806 (2006).
[20] P. D. D. Schwindt, S. Knape, A. Shah, L. Hollberg, and J. Kitching, Appl. Phys. Lett. **85**, 6409 (2004).
[21] C. Andreeva *et al.*, Appl. Phys. B: Lasers Opt. **76**, 667 (2003).
[22] A. Huss, R. Lammegger, L. Windholtz, E. Alipieva, S. Gateva, L. Petrov, E. Taskova, and G. Todorov, J. Opt. Soc. Am. B **23**, 1729 (2006).
[23] K. Nasyrov, S. Cartaleva, N. Petrov, V. Biancalana, Y. Dancheva, E. Mariotti, and L. Moi, Phys. Rev. A **74**, 013811 (2006).
[24] F. Renzoni, S. Cartaleva, G. Alzetta, and E. Arimondo, Phys. Rev. A **63**, 065401 (2001).
[25] G. Alzetta, S. Cartaleva, Y. Dancheva, Ch. Andreeva, S. Gozzini, L. Botti, and A. Rossi, J. Opt. B: Quantum Semiclassical Opt. **3**, 181 (2001).
[26] D. V. Brazhnikov, A. V. Taichenachev, A. M. Tumaikin, V. I. Yudin, S. A. Zibrov, Y. O. Dudin, V. V. Vasilev, and V. L. Velichansky, JETP Lett. **83**, 64 (2006).
[27] M. M. Mijailović, J. Dimitrijević, A. J. Krmpot, Z. D. Grujić, B. M. Panić, D. Arsenović, D. V. Pantelić, and B. M. Jelenković, Opt. Express **15**, 1328 (2007).
[28] M. L. Harris, C. S. Adams, S. L. Cornish, I. C. McLeod, E. Tarleton, and I. G. Hughes, Phys. Rev. A **73**, 062509 (2006).
[29] Janis Alnis and Marcis Auzinsh, J. Phys. B **34**, 3889 (2001).
[30] Ferruccio Renzoni and Ennio Arimondo, Phys. Rev. A **58**, 4717 (1998).
[31] J. Dimitrijević, D. Arsenović, and B. M. Jelenković, Phys. Rev. A **76**, 013836 (2007).
[32] G. Wasik, W. Gawlik, J. Zachorowski, and W. Zawadzki, Appl. Phys. B: Lasers Opt. **75**, 613 (2002).